Available online at www.sciencedirect.com
SCIENCE DIRECT®
Journal of volcanology and geothermal research
ELSEVIER
Journal of Volcanology and Geothermal Research 121 (2003) 115–135
www.elsevier.com/locate/jvolgeores

Late Mesozoic calc-alkaline volcanism of post-orogenic extension in the northern Da Hinggan Mountains, northeastern China

Wei-Ming Fan *, Feng Guo, Yue-Jun Wang, Ge Lin

Guangzhou Institute of Geochemistry, Chinese Academy of Sciences, Wushan, Guangzhou 510640, PR China

Received 25 March 2002; accepted 12 August 2002

Abstract

Late Mesozoic calc-alkaline volcanism in the northern Da Hinggan Mountains (NDHM), NE China, exhibits geochemical and Sr–Nd isotopic characteristics similar to those of Cenozoic calc-alkaline volcanism in the Basin and Range Province, USA. Whole-rock K–Ar dating results show that these volcanic sequences were erupted during 138–116 Ma, composed of basaltic andesites/trachyandesites (Group 1), hornblende andesites/trachytes (Group 2) and rhyolite lavas (Group 3). They are characterized by low MgO contents ($\leq 4.20\%$), LILE, LREE enrichment and significant Nb–Ta depletion, as well as a little depleted to slightly enriched Nd and weakly enriched Sr isotopic ratios (Group 1: initial $^{87}Sr/^{86}Sr = 0.70502–0.70572$; $\varepsilon_{Nd}(t) = -0.78$ to $+0.91$; Group 2: initial $^{87}Sr/^{86}Sr = 0.70497–0.70518$; $\varepsilon_{Nd}(t) = +0.86$ to $+1.26$; Group 3: initial $^{87}Sr/^{86}Sr = 0.70510–0.70635$; $\varepsilon_{Nd}(t) = -0.41$ to $+0.25$). The systematic variations in major and trace elements, homogeneous Sr–Nd isotope data and temporal consistency among three volcanic groups, indicate that they were derived from a similar mantle source metasomatized by fluids related to the closure of the paleo-Asian and/or Mongolia–Okhotsk Oceans, and were produced through different degrees of fractional crystallization of the primary melts. Group 1 basaltic rocks were formed through removal of olivine and pyroxene of the primary melts, while Group 2 trachytes, which contain the lowest LREE contents (e.g., La = 24–28 ppm) and relatively less enriched Sr and higher Nd isotope ratios, were generated after removal of a few percent of LREE-rich minerals such as hornblende, clinopyroxene and apatite of melts like Group 1. Group 3 rhyolite lavas exhibiting the highest abundances of strongly incompatible elements such as Rb and K, moderate LREE contents (e.g., La = 28–53 ppm) as well as apparently negative Eu and Sr anomalies, represent the final crystallized products following a plagioclase-predominant fractionation of melts like Group 2. The low MgO contents and evolved affinities of the volcanic rocks imply that beneath the NDHM there existed many crustal magma reservoirs throughout the eruption episodes, in which mantle-derived primary melts had experienced intense differentiation. These facts, in combination with the contemporaneous basin and range tectonic regime, suggest that the extensive calc-alkaline volcanism in the NDHM was attributed to post-orogenic diffuse extension rather than either an upwelling mantle plume or Mesozoic oceanic plate subduction.

Keywords: geochemistry; calc-alkaline volcanism; late Mesozoic; lithospheric extension; northeastern China

* Corresponding author. Tel.: +86-10-68-59-75-23; Fax: +86-10-68-59-75-83.
E-mail address: wmfan@cashq.ac.cn (W.-M. Fan).

0377-0273/02/$ – see front matter © 2002 Elsevier Science B.V. All rights reserved.
PII: S0377-0273(02)00415-8

1. Introduction

Certain igneous rock suites are closely associated with particular tectonic settings, and a large number of studies have sought to investigate the causes of melt generation in different tectonic settings. For instance, calc-alkaline volcanism has been usually considered to occur in destructive plate margins, where the mantle has been chilled by subduction of oceanic crust, and magma generation is attributed to lowering of the peridotite solidus by introduction of H_2O and other volatiles from the subducted slabs (Gill, 1981; Grove and Kinzler, 1986; Davies and Stevenson, 1992; Arculus, 1994). However, more and more evidence suggests that calc-alkaline melts also may be formed in areas of extension as a consequence of post-orogenic or post-collisional stress relaxation (Hawkesworth et al., 1995; Hooper et al., 1995; Rogers et al., 1995; Turner et al., 1996; Liegéois et al., 1998; Rotturaa et al., 1998; Miller et al., 1999; Guo et al., 2001; Fan et al., 2001). Comparative studies between intracontinental and island arc calc-alkaline volcanics reveal that intraplate calc-alkaline volcanic rocks are generated through partial melting of lithospheric mantle that had been modified during previous subduction, exhibiting some geochemical differences from island arc volcanics (e.g., Hawkesworth et al., 1995; Turner et al., 1996; Jahn et al., 1999; Miller et al., 1999).

The NE China fold belt is the eastern segment of the gigantic accreting continental margin of the Mongolia–Okhotsk orogenic belt (Sëngor et al., 1993; Sëngor and Natal'in, 1996), in which late Mesozoic volcanic rocks are widely distributed. The volcanic sequences were mainly erupted during late Jurassic to early Cretaceous after the final collision between the Siberia Craton and the North China–Mongolian block (Zhao et al., 1990, 1994; BGMRNM, 1991, 1996; Zhao and Coe, 1996; van der Voo et al., 1999), accompanied by basin and range tectonics (Li and Yang, 1987; Shao et al., 1994; Guo et al., 2001). These rocks generally exhibit calc-alkaline to high-K calc-alkaline affinities and their petrogenesis remains controversial. A mantle plume hypothesis has been proposed to interpret the extensive late Mesozoic magmatism in Da Hinggan Mountains (NDHM) (Lin et al., 1998; Ge et al., 1999), whereas an active continental margin related to the Mesozoic subduction of the Kula or Izanagi Plate has also been put forward (Jiang and Quan, 1988; Zhao et al., 1989, 1994; Faure and Natal'in, 1992; Xia et al., 1993). In order to characterize the late Mesozoic volcanic rocks in the NDHM, here we report K–Ar dating results, major and trace element geochemistry, and Sr and Nd isotope data for the successive volcanic sequences. The purpose of this paper is to understand the source characteristics and petrogenesis of these volcanic rocks as well as the extensional mechanism for the widespread melting event.

2. Background geology and petrography

The NDHM are located in NE China, south of the suture between the North China–Mongolian Block and the Siberia Craton and north of the Solonker–Xilinhot–Hegenshan fault (Fig. 1) believed to mark the subduction zone along the northern margin of North China block during the late Paleozoic (Sëngor et al., 1993). The Paleozoic strata, which are mainly composed of low-grade metamorphic volcano-sedimentary associations, epipelagic limestones, and clastic rocks, are sporadically exposed and intruded by voluminous Hercynian–early Yanshanian granitic plutons. Along the lithosphere-scale faults are widely distributed ophiolite suites and tectonic nappes of different ages (Fig. 1), suggesting that multi-stage oceanic subduction and continent–arc collision occurred during the closure of the paleo-Asian and Mongolia–Okhotsk Oceans. Paleogeographic reconstruction indicates that the orogenic belt had been entirely uplifted by the end of the late Carboniferous due to extensive emplacement of Hercynian granitic plutons (BGMRNM, 1991). These intrusions, together with early Yanshanian granitoids, have positive ε_{Nd} values that suggest that the NE China Fold belt is also an important area for Phanerozoic continental crustal growth (Hong et al., 1994; Han et al., 1997; Wu et al., 1997, 2000; Chen et al., 2000).

Paleomagnetic evidence and geophysical obser-

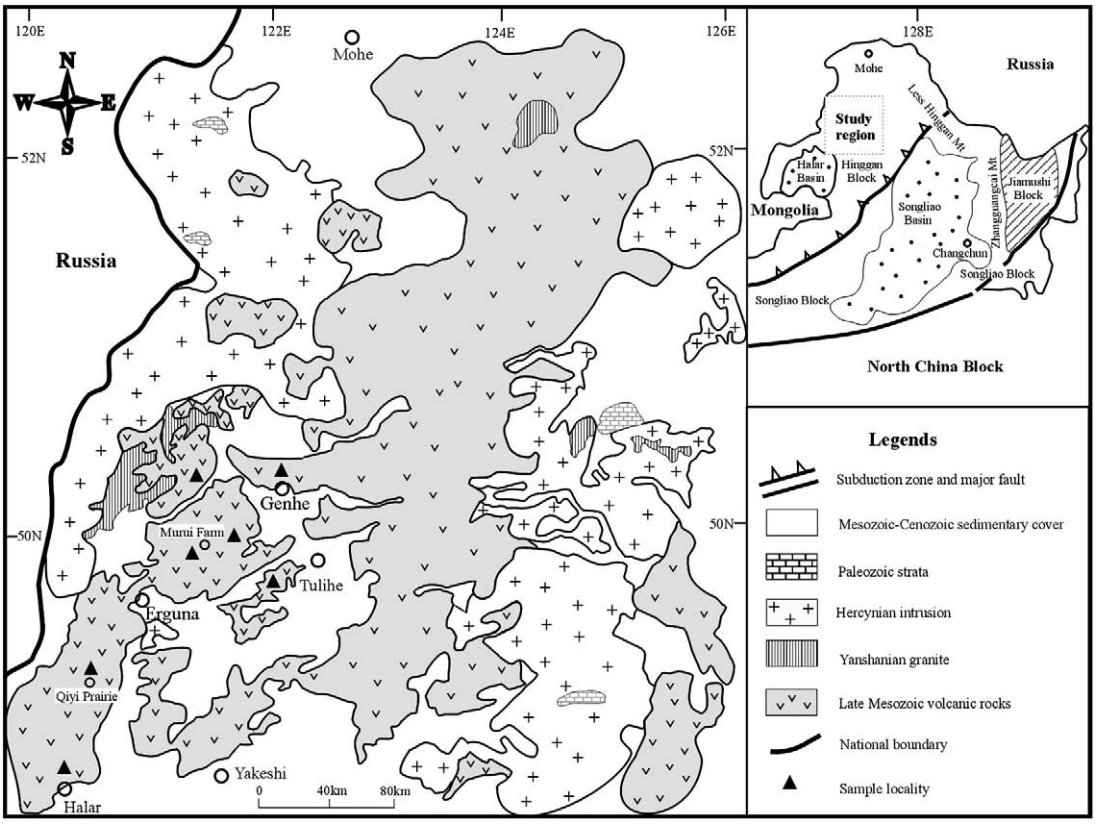

Fig. 1. Simplified tectonic map and distribution of late Mesozoic volcanic rocks in NDHM, NE China (after BGMRNM, 1991).

vations imply that the ultimate collision event between the North China–Mongolian Block and the Siberia Craton took place no later than the middle Jurassic (Zhao et al., 1990; Zhao and Coe, 1996; Kuzmin et al., 1996; van der Voo et al., 1999). During the late Mesozoic, regional tectonic activity was dominated by faulting and rifting (Li and Yang, 1987), triggering the formation of basin and range tectonics and accompanied by extensive calc-alkaline magmatism.

The NDHM are widely covered by late Mesozoic volcanic rocks (Fig. 1, BGMRNM, 1991), which comprise a wide spectrum of rock types, including basaltic trachyandesite, trachyandesite, trachyte, and rhyolite lava flows and rhyolitic tuff. On the basis of lithological associations and temporary relationships, we divide the studied volcanic sequences into three groups.

Samples in Tamulangou Fm. (termed Group 1) were collected at Murui Farm and Qiyi Prairie, composed mainly of basaltic trachyandesites and trachyandesites. They are commonly subaphyric to weakly porphyritic with predominant phenocrysts of pyroxene of 1–3 mm with rare olivine and plagioclase found. The matrix is mainly composed of fine-grained or aphanitic clinopyroxene and plagioclase (<0.2 mm) and a few opaque oxides.

The volcanic rocks in Jixiangfeng Fm. (termed Group 2) were sampled about 4 km north of Genhe town along the railway profile. The volcanic sequences exhibit a columnar joint and comprise mainly hornblende trachytes with minor pyroclastic tuffs. These rocks generally show a porphyritic fabric with phenocrysts of hornblende and plagioclase of 4–7 mm grain sizes. The matrix includes

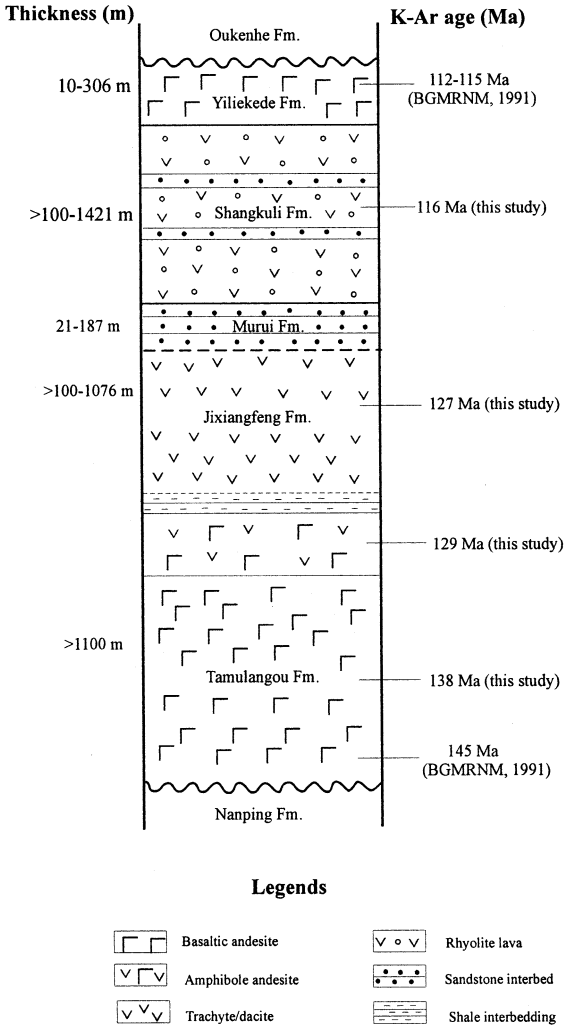

Fig. 2. Late Mesozoic volcano-sedimentary column and volcanic eruption ages in the NDHM. The thickness of volcano-sedimentary sequences is from BGMRNM (1991, 1996).

fine-grained plagioclase and hornblende of 0.2–0.5 mm and a few opaque oxides.

Samples of Shangkuli Fm. (termed Group 3) were mainly gathered adjacent to Halar and Tulihe towns (Fig. 1). The volcanic sequence occurs in subparallel layers with tuffecous sandstone interbeddings in rhyolitic lavas. The rhyolites show a subaphyric to weakly porphyritic texture with a few phenocrysts of quartz and biotite of about 2–3 mm. A detailed description of field relationships among these volcanic sequences, and their eruption ages, are illustrated in Fig. 2.

3. Analytical techniques

All samples were crushed to about mm-scale grain size after removal of weathered rims and handpicked under a magnifier to exclude xenocrysts and amygdaloid. Only fresh and xenocryst- and amygdaloid-free rock chips were selected. These slips were washed in purified water in an ultrasonic bath and crushed in a WC jaw crusher. A split was ground to <160 mesh grain size in an agate ring mill, and this material was used for major and trace element analyses. Major element analysis was carried out by a traditional wet chemical method at Changsha Institute of Geotectonics, Chinese Academy of Sciences (CAS). The analytical errors for major oxides are less than 2%. Trace element ICP-MS analysis was performed at Guangzhou Institute of Geochemistry, CAS. The detailed analytical procedure follows that reported by Liu et al. (1996). Reproducibility is better than 95%, and the analytical error for most of the trace elements is less than 5% and about 10% for Ni, Sc, and V.

Sr and Nd isotopic ratios were measured at the Institute of Geology and Geophysics, CAS. Rock chips of <20 mesh are applied to perform Sr and Nd isotope analysis. Before being ground to <160 mesh in an agate rill mill and dissolved, these chips were leached in purified 6 N HCl for 24 h at room temperature to avoid the influence of surface alteration or weathering, especially for Sr isotopic ratios. The Sr and Nd isotope ratios were respectively normalized to $^{86}Sr/^{88}Sr = 0.1194$ and $^{146}Nd/^{144}Nd = 0.7219$. The La Jolla standard yielded $^{143}Nd/^{144}Nd = 0.511862 \pm 10$ ($n = 13$) and NBS987 gave $^{87}Sr/^{86}Sr = 0.710240 \pm 11$ ($n = 6$). The whole procedure blank is less than $2–5 \times 10^{-10}$ g for Sr and 5×10^{-11} g for Nd. Analytical errors for Sr and Nd isotopic ratios were given as 2σ. The $^{87}Rb/^{86}Sr$ and $^{147}Sm/^{144}Nd$ ratios were calculated using the Rb, Sr, Sm and Nd abundance obtained by ICP-MS. The initial $^{87}Sr/^{86}Sr$ and $^{143}Nd/^{144}Nd$ ratios were corrected using their whole-rock mean K–Ar ages of 135 Ma for Tamulangou Fm., 127 Ma for Jixiangfeng Fm., and 116 Ma for Shangkuli Fm.

K–Ar dating was performed at Guangzhou Institute of Geochemistry, CAS. Except for horn-

Table 1
Major oxide contents (in wt%) of late Mesozoic volcanics in the NDHM, NE China

Group	Sample	Location	Age (Ma)	SiO_2	Al_2O_3	Fe_2O_3	FeO	CaO	MgO	K_2O	Na_2O	P_2O_5	MnO	TiO_2	LOS	Total	Mg#
Group 1 (Tamulangou Fm.)	HLR-11	Qiyi Prairie	129.5 ± 2.0	56.82	17.63	3.43	2.82	6.09	3.81	1.84	3.69	0.38	0.08	1.03	2.86	100.48	0.54
	HLR-13	Qiyi Prairie		55.74	17.97	3.65	3.06	6.83	2.50	1.91	4.19	0.40	0.11	1.07	2.64	100.07	0.41
	HLR-19	Qiyi Prairie		54.86	17.23	3.03	3.38	6.89	2.59	1.69	4.14	0.37	0.09	1.00	3.92	99.19	0.43
	EGN-19	Murui Farm	126.1 ± 2.0	55.22	17.70	6.47	1.27	6.63	1.45	1.83	3.97	0.62	0.11	1.36	3.08	99.71	0.27
	EGN-20	Murui Farm		56.12	17.50	5.80	1.27	6.22	2.27	2.18	4.02	0.62	0.12	1.28	2.26	99.66	0.39
	EGN-21	Murui Farm		55.82	17.43	5.80	1.00	6.83	1.82	2.42	4.27	0.62	0.12	1.31	2.50	99.94	0.34
	EGN-24	Murui Farm		56.68	17.91	6.04	1.32	4.46	1.77	2.45	5.32	0.58	0.10	1.23	2.32	100.18	0.32
	EGN-26	Murui Farm		52.66	17.50	6.51	1.61	5.75	2.73	2.79	4.00	0.82	0.13	1.49	3.32	99.31	0.40
	EGN-27	Murui Farm		54.34	17.70	5.80	1.04	4.60	1.82	3.06	4.29	0.72	0.12	1.52	4.78	99.79	0.34
	EGN-28	Murui Farm		54.40	17.23	5.34	1.83	7.71	2.41	1.95	3.90	0.58	0.16	1.28	3.24	100.03	0.40
	EGN-29	Murui Farm		54.68	17.23	4.63	2.36	7.44	2.73	2.05	4.09	0.60	0.13	1.26	2.24	99.44	0.43
	EGN-30	Murui Farm		51.62	17.57	7.50	1.20	7.57	2.73	1.51	4.01	0.68	0.10	1.54	3.60	99.63	0.38
	EGN-31	Murui Farm		52.10	17.50	6.25	2.98	3.38	4.00	1.68	5.00	0.69	0.11	1.58	3.84	99.11	0.46
	EGN-32	Murui Farm	138.5 ± 2.2	51.36	17.59	5.85	2.19	8.38	2.73	1.66	4.00	0.62	0.12	1.53	4.08	100.11	0.40
	EGN-34	Murui Farm		57.60	17.31	4.01	1.76	4.87	1.68	1.32	5.22	0.48	0.11	1.11	4.70	100.17	0.36
	EGN-35	Murui Farm		54.30	18.87	5.41	0.80	5.81	2.86	1.56	4.20	0.47	0.10	1.20	4.52	100.10	0.48
Group 2 (Jixiangfeng Fm.)	GH-5	Genhe		63.26	17.45	2.05	1.36	5.41	1.18	0.90	4.44	0.20	0.11	0.53	3.46	100.35	0.40
	GH-8	Genhe	126.9 ± 2.0	64.22	17.38	2.05	1.36	4.33	1.41	2.53	4.66	0.19	0.10	0.50	1.86	100.59	0.44
	GH-10	Genhe		65.68	16.77	2.65	0.62	3.58	1.18	4.62	3.65	0.19	0.10	0.52	1.02	100.58	0.41
	GH-12	Genhe		64.32	17.25	2.45	1.02	3.92	1.27	4.89	3.62	0.20	0.09	0.49	1.10	100.62	0.41
	GH-14	Genhe		64.96	17.18	2.10	1.26	3.99	1.18	1.81	5.50	0.19	0.11	0.48	1.54	100.30	0.40
	GH-15	Genhe		65.70	16.77	2.28	0.84	3.52	0.91	4.26	4.76	0.18	0.14	0.51	0.86	100.73	0.36
	GH-16	Genhe		63.40	16.84	2.43	0.89	3.38	1.27	3.10	4.76	0.19	0.09	0.47	3.40	100.22	0.43
	GH-19	Genhe		66.80	16.23	2.52	0.77	3.79	0.91	3.33	4.70	0.18	0.10	0.51	0.82	100.66	0.35
	GH-28	Genhe		60.96	17.25	4.10	1.11	4.73	1.27	3.02	4.89	0.26	0.17	0.47	1.88	100.11	0.32
Group 3 (Shangkuli Fm.)	EGN-12	Halar		71.48	15.15	1.19	0.38	1.76	0.91	5.52	3.70	0.06	0.04	0.25	0.24	100.68	0.53
	EGN-14	Halar		70.06	15.29	0.95	0.62	1.83	0.73	5.80	3.78	0.06	0.07	0.26	0.52	99.97	0.47
	YTH-1	Tulihe		74.04	13.53	0.55	0.57	1.49	0.82	5.00	3.52	0.02	0.08	0.13	1.06	100.81	0.58
	YTH-2	Tulihe		76.32	13.12	0.49	0.57	1.01	0.45	4.52	3.19	0.01	0.05	0.13	0.78	100.64	0.44
	YTH-4	Tulihe		74.10	14.07	0.51	0.46	1.01	1.00	5.04	3.51	0.01	0.05	0.12	0.82	100.70	0.66
	YTH-8	Tulihe	116.4 ± 1.8	76.44	12.58	0.51	0.44	1.35	0.45	4.10	3.52	0.02	0.05	0.12	0.80	100.38	0.47
	YTH-13	Tulihe		75.16	12.85	0.58	0.44	1.35	0.64	4.75	3.23	0.01	0.04	0.11	0.76	99.92	0.54
	YTH-26	Tulihe		75.42	12.98	0.76	0.37	0.95	0.45	4.19	3.74	0.01	0.04	0.13	0.50	99.54	0.43
	YTH-28	Tulihe		75.92	13.12	0.72	0.39	1.22	0.45	4.61	3.29	0.01	0.03	0.11	0.56	100.43	0.44
	YTH-29	Tulihe		74.92	12.72	0.62	0.36	1.22	0.41	4.79	3.82	0.01	0.03	0.10	0.58	99.58	0.45

Table 2
Trace element contents (in ppm) and Sr–Nd isotope data of late Mesozoic volcanic rocks in the NDHM, NE China

Formation	Tamulangou (Group 1)											
Sample	EGN-19	EGN-20	EGN-21	ENG-24	ENG-26	ENG-28	ENG-30	ENG-32	ENG-34	HLR-11	HLR-13	HLR-19
Age (Ma)	126.1 ± 2.0							138.5 ± 2.2		129.5 ± 2.0		
Sc	11.49	10.61	10.28	10.50	9.23	9.15	9.41	11.41	10.24	9.01	9.46	9.20
V	145.9	133.2	134.1	123.4	142.9	134.3	193.1	180.0	116.1	122.4	127.2	115.5
Co	19.90	20.47	20.71	16.01	23.59	24.46	23.06	34.15	19.66	18.66	22.08	20.54
Ni	31.92	28.42	30.66	24.85	24.34	39.06	38.76	50.17	34.59	34.88	40.35	38.34
Rb	45.18	51.81	55.72	48.26	62.88	77.95	42.62	51.46	47.31	45.59	40.08	38.08
Sr	1143	1019	1071	1379	1195	1103	1112	1122	770	1095	1060	1023
Ba	1223	964.4	1054	1635	1373	958.8	851.8	847.9	790.6	911.8	806.5	753.7
Nb	11.35	10.68	10.69	10.49	17.89	11.63	10.35	9.96	7.85	5.99	5.61	5.72
Ta	0.70	0.63	0.66	0.66	1.21	0.82	0.66	0.68	0.51	0.44	0.41	0.43
Th	5.55	5.32	5.22	6.09	12.74	10.23	7.52	8.97	5.76	4.82	4.55	4.53
U	1.29	1.19	1.21	1.25	3.01	2.64	1.57	1.64	1.39	1.39	1.33	1.36
Zr	327.8	307.7	300.7	339.5	318.4	237.5	240.7	230.5	246.2	203.3	192.0	197.5
Hf	8.46	7.77	8.23	8.65	8.21	7.00	6.42	6.49	6.46	5.73	5.65	5.57
Y	19.15	17.96	18.46	16.84	24.79	19.33	18.63	19.24	15.96	15.59	14.88	15.30
La	63.41	57.03	59.90	58.68	69.52	51.99	48.53	48.29	44.20	30.76	29.38	28.55
Ce	137.6	131.8	129.5	132.9	147.5	116.8	109.9	109.5	91.20	72.58	69.75	65.00
Pr	16.41	15.35	16.11	15.58	18.48	14.23	13.71	14.19	12.34	8.82	8.68	8.51
Nd	57.79	54.06	55.47	54.25	61.33	48.83	49.15	50.86	43.61	31.76	32.90	30.92
Sm	10.19	9.66	9.81	9.93	11.65	9.43	9.46	9.60	8.25	6.55	6.55	6.18
Eu	2.70	2.55	2.58	2.60	2.82	2.43	2.65	2.75	2.48	1.97	1.90	1.88
Gd	8.89	8.09	8.74	8.06	10.17	8.89	8.13	8.47	7.24	5.77	5.64	5.61
Tb	0.97	0.89	0.92	0.88	1.15	0.95	0.95	0.95	0.78	0.66	0.68	0.67
Dy	4.31	4.20	4.12	3.77	5.27	4.38	4.27	4.52	3.54	3.27	3.23	3.35
Ho	0.72	0.70	0.71	0.68	0.92	0.75	0.70	0.75	0.62	0.59	0.60	0.56
Er	1.92	1.81	1.80	1.73	2.39	1.88	1.81	1.88	1.54	1.55	1.53	1.54
Tm	0.25	0.24	0.24	0.24	0.29	0.26	0.23	0.25	0.21	0.23	0.21	0.22
Yb	1.47	1.52	1.51	1.49	2.01	1.64	1.43	1.52	1.31	1.44	1.42	1.45
Lu	0.20	0.21	0.21	0.19	0.28	0.23	0.20	0.21	0.18	0.20	0.20	0.21
δEu	0.85	0.86	0.84	0.86	0.77	0.80	0.90	0.91	0.96	0.96	0.93	0.96
$^{87}Rb/^{86}Sr$		0.1475	0.1509		0.1526		0.1111	0.1329	0.1782	0.1207		0.1079
$^{87}Sr/^{86}Sr$ ± 2σ		0.705445 ± 14	0.705834 ± 14		0.705566 ± 13		0.705405 ± 12	0.705584 ± 12	0.706073 ± 17	0.705240 ± 13		0.705222 ± 14
$^{87}Sr/^{86}Sr(i)$		0.705150	0.70553		0.70526		0.70518	0.705320	0.705720	0.70502		0.705020
$^{147}Sm/^{144}Nd$		0.1081	0.1070		0.1148		0.1163	0.1141	0.1144	0.1252		0.1209
$^{143}Nd/^{144}Nd$ ± 2σ		0.512580 ± 9	0.512559 ± 8		0.512523 ± 12		0.512571 ± 8	0.512579 ± 6	0.512609 ± 10	0.512621 ± 6		0.512602 ± 8
$\varepsilon_{Nd}(t)$		0.45	0.06		−0.78		0.13	0.32	0.91	0.85		0.55

The initial Sr and Nd isotope ratios for the three groups of volcanic rocks are corrected by K–Ar ages of 135 Ma, 127 Ma and 116 Ma, respectively. $^{87}Rb/^{86}Sr$ and $^{147}Sm/^{144}Nd$ ratios are calculated using the Rb, Sr, Sm and Nd contents obtained by ICP-MS analysis.

Table 2 (*Continued*).

Formation	Group 2 (Jixiangfeng Fm.)					Group 3 (Shangkuli Fm.)				
Sample	GH-5	GH-10	GH-16	GH-19	GH-28	EGN-12	EGN-14	YTH-1	YTH-8	YTH-28
Age (Ma)		126.9 ± 2.0							116.4 ± 1.8	
Sc	3.47	3.31	3.00	3.66	9.41	3.54	3.97	0.91	0.79	0.70
V	35.23	34.10	33.47	33.49	80.54	7.70	8.19	4.95	4.48	4.39
Co	4.50	7.96	4.28	6.05	9.97	5.81	3.31	2.08	1.80	1.63
Ni	0.90	0.62	0.74	0.66	2.60	0.20	0.06	0.45	0.08	0.29
Rb	29.81	107.5	93.17	85.22	73.58	241.4	231.1	213.1	168.8	189.4
Sr	1467	533.0	538.2	631.0	608.1	113.1	131.4	69.9	91.30	72.80
Ba	809.0	1008	963.6	1119	1044	617.8	669.1	251.0	259.5	202.0
Nb	6.22	6.16	6.23	6.10	5.52	14.94	14.50	12.81	10.93	11.39
Ta	0.60	0.59	0.59	0.57	0.52	1.34	1.27	1.33	1.18	1.13
Th	9.22	9.45	9.68	9.14	8.09	27.73	25.75	28.10	24.30	23.75
U	3.30	3.23	3.25	3.07	2.86	3.10	4.30	5.74	6.01	5.50
Zr	199.3	196.5	190.9	190.5	155.4	158.3	146.0	128.3	110.3	102.4
Hf	5.71	5.74	5.73	5.59	4.88	5.80	5.42	5.35	4.78	4.48
Y	18.77	17.69	17.65	17.33	19.50	23.40	25.22	18.26	17.00	15.21
La	27.21	26.74	27.12	28.07	23.86	42.44	53.46	34.11	33.40	28.17
Ce	58.16	58.83	58.58	60.60	51.84	80.23	111.96	74.03	69.27	60.10
Pr	7.19	7.05	6.68	6.75	6.51	10.65	12.47	7.98	7.79	6.53
Nd	24.15	23.18	24.13	23.41	23.73	33.43	40.38	23.53	23.30	18.83
Sm	4.96	4.93	4.74	4.76	4.91	6.44	7.63	4.64	4.39	3.80
Eu	1.39	1.44	1.33	1.31	1.46	1.12	1.29	0.51	0.51	0.40
Gd	4.88	4.65	4.62	4.59	5.07	5.86	7.13	4.28	4.10	3.50
Tb	0.62	0.64	0.58	0.57	0.67	0.80	0.92	0.59	0.56	0.49
Dy	3.47	3.45	3.37	3.19	3.70	4.31	4.91	3.30	3.12	2.67
Ho	0.68	0.69	0.69	0.62	0.75	0.88	0.93	0.64	0.59	0.52
Er	1.94	1.86	1.83	1.82	1.98	2.45	2.67	1.80	1.65	1.45
Tm	0.31	0.31	0.30	0.29	0.30	0.40	0.43	0.30	0.27	0.24
Yb	2.12	2.08	2.11	2.00	2.03	2.88	3.00	2.02	1.79	1.66
Lu	0.34	0.33	0.33	0.30	0.30	0.42	0.44	0.29	0.26	0.24
δEu	0.85	0.91	0.86	0.85	0.89	0.55	0.53	0.35	0.36	0.33
$^{87}Rb/^{86}Sr$		0.5848	0.5019	0.2654	0.3508	6.1884	5.0973	8.8400	5.3589	
$^{87}Sr/^{86}Sr$ ±2σ		0.706065 ± 13	0.705872 ± 10		0.705657 ± 9	0.705612 ± 13	0.715215 ± 23	0.713957 ± 10	0.720923 ± 19	0.714545 ± 12
$^{87}Sr/^{86}Sr(i)$		0.705010	0.70497	0.70518	0.704980	0.705010	0.705550	0.70635	0.705710	
$^{147}Sm/^{144}Nd$		0.1287	0.1187	0.1230	0.1250	0.1164	0.1142	0.1192	0.1140	
$^{143}Nd/^{144}Nd$ ±2σ		0.512645 ± 8	0.512637 ± 11		0.512621 ± 7	0.512643 ± 8	0.512590 ± 7	0.512583 ± 9	0.512558 ± 9	0.512566 ± 8
$\varepsilon_{Nd}(t)$		1.24	1.24	0.86	1.26	0.25	0.15	−0.41	−0.18	

blende andesites and dacites that exhibit porphyritic fabrics, only glassy or aphanitic samples were selected for K–Ar analysis. Rock slips were crushed to 0.2–0.9 mm grain size. ^{38}Ar diluent was added after the samples were entirely molten at 1300°C in a vacuum Ar extraction system at 10^{-9}–10^{-10} mbar. Released gases from the molten samples were purified with Ti spongy. Then a Ti evaporated pump and a Zr–Al pump were used in turn to further purify the Ar gas. Finally, the purified Ar gas was collected using a 'C-shape' pipe at a temperature below liquid nitrogen and the Ar content measured by a mass spectrum MM-1200. K contents were measured by atomic absorption. Age calculation parameters used in this paper are: $K^{40} = 0.1167\%$, $K_e = 5.811 \times 10^{-11}$/yr, $K_b = 4.962 \times 10^{-10}$/yr. The analytical result for Chinese standard ZBH-2506 is

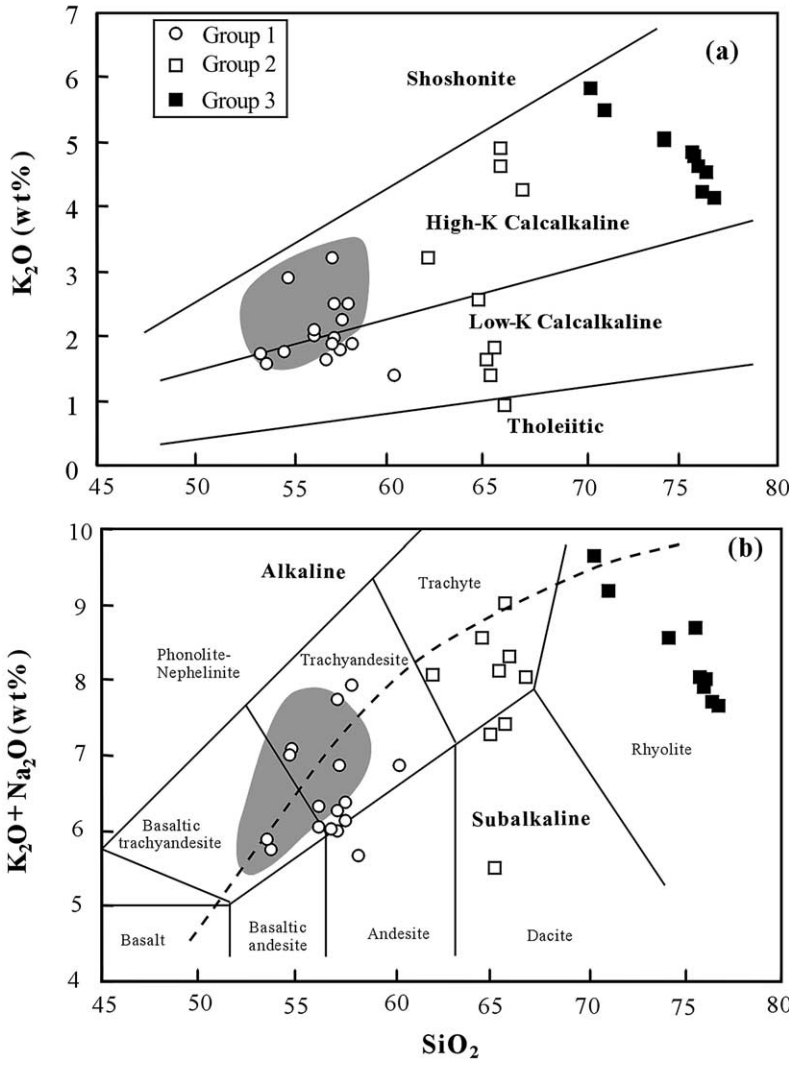

Fig. 3. K_2O–SiO_2 (a) and TAS (b) plots of the late Mesozoic volcanic rocks in the NDHM (Le Bas et al., 1986). Note that all of the volcanic rocks in NDHM show calc-alkaline to high-K calc-alkaline characters. The boundary between alkaline and subalkaline series is from Irvine and Baragar (1971). The shaded area denotes the variation range of late Mesozoic basaltic lavas in the NDHM (Ge et al., 1999). Symbols as shown in the figure.

132.32 ± 2.09 Ma (its international recommended age is 132.0 Ma). K–Ar dating results, major and trace element compositions and Sr and Nd isotope data are listed in Tables 1 and 2.

4. Results

4.1. K–Ar dating

Five fresh samples with weakly porphyritic to aphyric fabrics were selected to perform K–Ar dating for determining the eruption ages of the late Mesozoic volcanic rocks. Three basaltic trachyandesite samples respectively from the lower, middle, and upper segments of the Tamulangou Fm. gave K–Ar apparent ages of 138.5 ± 2.2 Ma, 129.5 ± 2.0 Ma and 126.1 ± 2.0 Ma. These dating results are in good agreement with the K–Ar age range (145–126 Ma) of most of the previous studies on Tamulangou Fm. (BGMRNM, 1991). One trachyte sample from the Jixiangfeng Fm. and one rhyolite sample from Shangkuli Fm., respectively, gave K–Ar apparent ages of 126.9 ± 2.0 Ma and 116.4 ± 1.8 Ma. All of the K–Ar ages are consistent with the field relations shown in Fig. 2.

4.2. Major and trace elements

The late Mesozoic volcanic rocks in the NDHM are calc-alkaline (Fig. 3a) and plot as basaltic trachyandesites and trachyandesites (Group 1), trachytes and dacites (Group 2), and rhyolites (Group 3) in the TAS figure (Fig. 3b). Group 1 samples span a range of 53.48–60.33% SiO_2 with MgO of 1.50–4.20%, Group 2 62.16–66.91% SiO_2 and 0.91–1.43% MgO, Group 3 70.45–76.76% SiO_2 and 0.41–1.0% MgO. Low MgO (0.41–4.20%) and compatible element contents (Ni = 0.06–50.17 ppm, Co = 1.63–34.15 ppm and V = 4.39–193.1 ppm) indicate that these volcanics are all differentiates of parental melts.

A clear differentiation trend among three groups of rocks is observed in the SiO_2 vs. major and trace element variation diagrams (Fig. 4). There is a negative correlation between SiO_2 and MgO, FeO* (total FeO = FeO+Fe_2O_3), CaO, P_2O_5, TiO_2, V, Ni, Co, Zr. K_2O and Rb generally increase following the increase in SiO_2 for Group 1 and 2 samples but decrease for Group 3 (Figs. 3a and 4k). Ba and Al_2O_3 contents vary slightly from Group 1 to Group 2 while they rapidly decrease toward Group 3 (Fig. 4c,j).

Group 1 possesses the highest REE contents (ΣREE = 154.7–333.8 ppm, average 248.3 ppm) and Group 2 the lowest (ΣREE = 127.1–138.3 ppm, average 135.1 ppm). In the chondrite-normalized REE patterns (Fig. 5), all three groups exhibit LREE enrichment with similar LREE fractionation (La/Sm_{CN} = 2.83–4.79). Group 1 rocks are characterized by the highest LREE/HREE ratios (La/Yb_{CN} = 13.91–29.15, average 21.80) and the strongest HREE fractionation (Gd/Yb_{CN} = 3.14–4.90; average 4.17) compared with Group 2 trachytes (La/Yb_{CN} = 7.94–9.48, average 8.69; Gd/Yb_{CN} = 1.77–2.02, average 1.87) and Group 3 rhyolites (La/Yb_{CN} = 9.95–12.61, average 11.49; Gd/Yb_{CN} = 1.65–1.93, average 1.77). Group 1 and Group 2 display slightly negative Eu anomalies (Eu*/Eu = 0.77–0.96 for Group 1 and Eu*/Eu = 0.85–0.91 for Group 2) whereas Group 3 has significantly negative Eu anomalies (Eu*/Eu = 0.33–0.55).

In the primitive mantle (PM)-normalized spidergrams (Fig. 5), all of the samples display LILE, LREE enrichment and significant Nb–Ta depletion, completely different from MORB, OIB and CFB that show no or insignificant HFSE anomalies (Smedley, 1986; Sun and McDonough, 1989). With regard to Sm, Zr and Hf anomalies are negligible, whereas Ba, Sr, P, and Ti anomalies vary from Group 1 through Group 2 to Group 3. For instance, Ba and Sr vary from positive anomalies in Group 1 through insignificant anomalies in Group 2 to strongly negative anomalies in Group 3. Ti and P depletion is observed in Group 2 and Group 3 rocks but is insignificant in Group 1 samples.

All three groups generally have much higher Ba/La and lower Nb/La ratios than those of MORB, OIB and intraplate basalts (Sun and McDonough, 1989). When plotted in the Ba/Nb versus Nb/La diagram (Fig. 6), they overlap the variation range of orogenic andesites. Additionally, Groups 1 and 2 show similar Sr contents and Zr/Y ratios to those of Cenozoic calc-alkaline

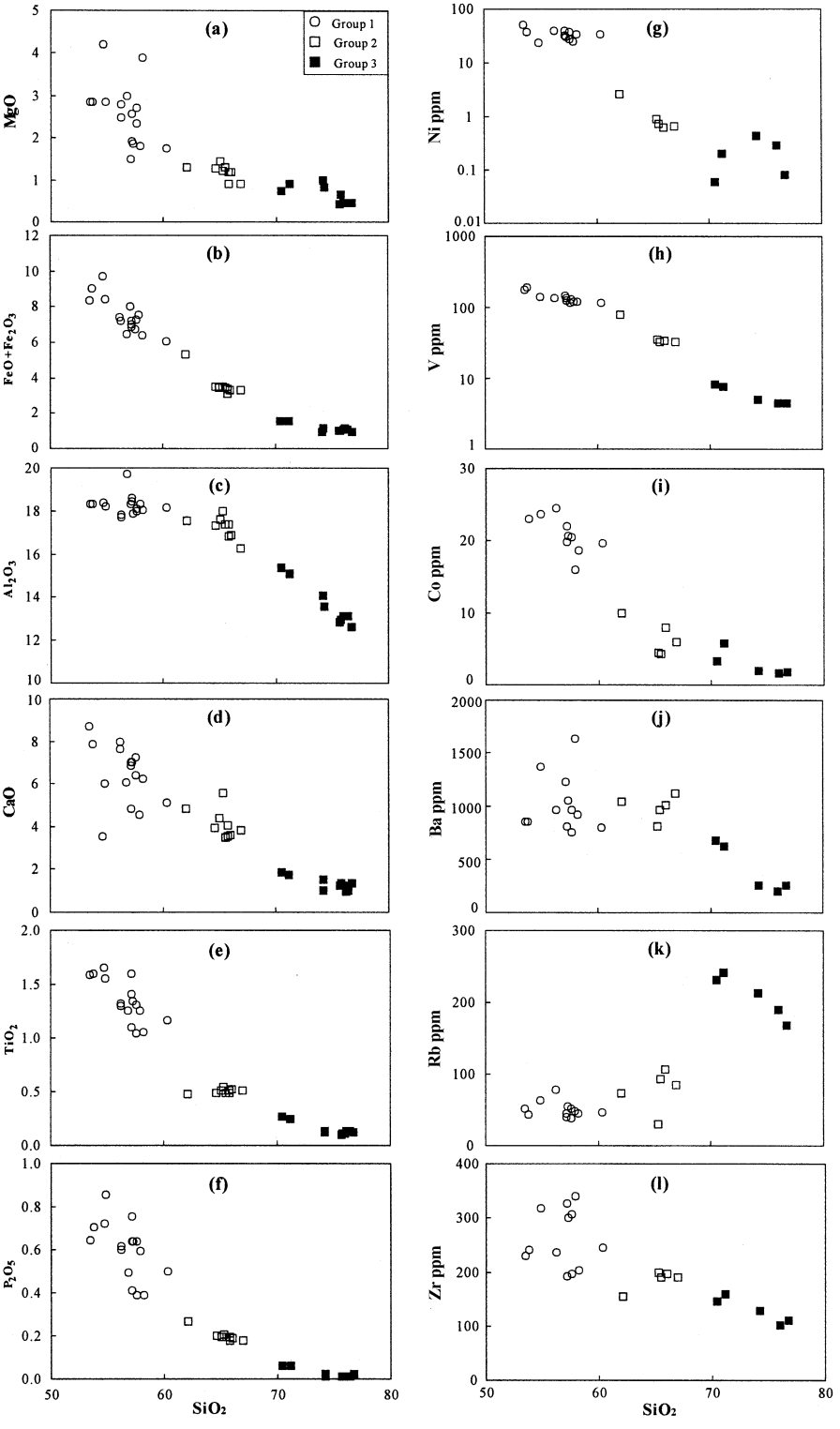
(a)
Group 1
Group 2
Group 3
MgO
(b)
FeO+Fe2O3
(c)
Al2O3
(d)
CaO
(e)
TiO2
(f)
P2O5
SiO2
(g)
Ni ppm
(h)
V ppm
(i)
Co ppm
(j)
Ba ppm
(k)
Rb ppm
(l)
Zr ppm
SiO2

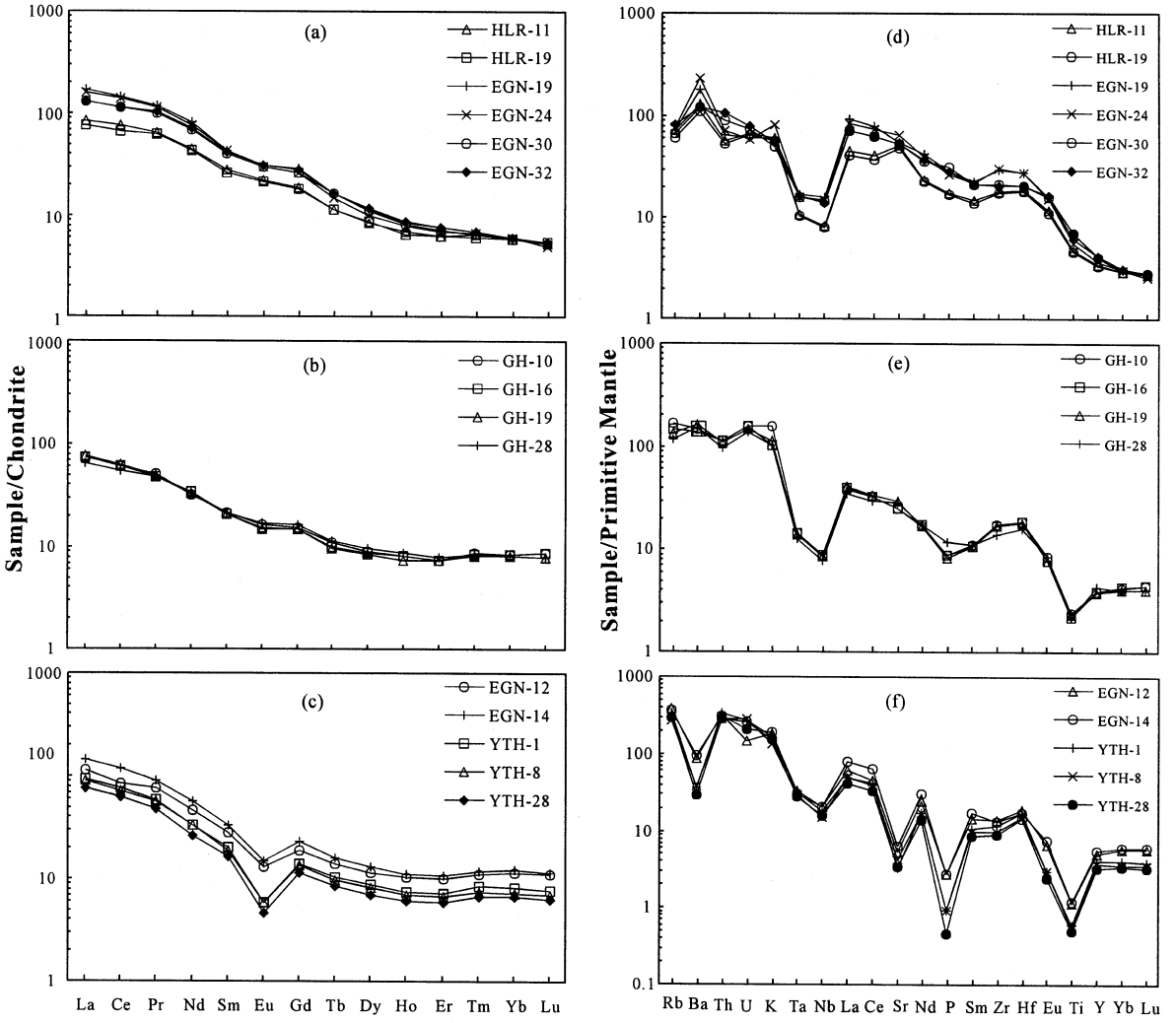

Fig. 5. Chondrite-normalized REE patterns (a–c) and primitive mantle-normalized spidergrams (d–f) of the late Mesozoic volcanic rocks in the NDHM. Chondrite values are from Taylor and McLennan (1985); primitive mantle value is from Sun and McDonough (1989).

volcanics of the Basin and Range Province (BRP) but have much higher Sr contents and Zr/Y ratios than those of island arc volcanics as illustrated in Fig. 7a,b (Hawkesworth et al., 1995; Hunter and Blake, 1995).

4.3. Sr and Nd isotope data

All of the late Mesozoic volcanic rocks in the NDHM display very similar initial Sr and Nd isotopic ratios despite their lithological differences

Fig. 4. Harker diagrams of the late Mesozoic volcanic rocks in the NDHM. A clear magma differentiation trend is displayed among Groups 1, 2 and 3. All major oxides are loss-free normalized to 100%. Symbols as in Fig. 3.

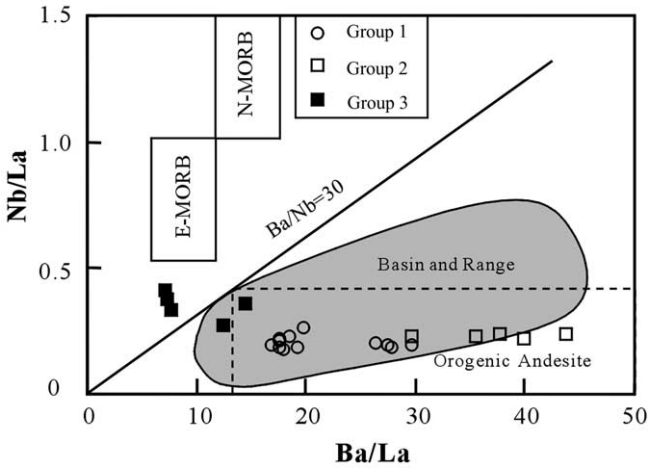

Fig. 6. Ba/La vs Nb/La variation diagrams of the late Mesozoic volcanic rocks. All samples have lower Nb/La ratios but higher Ba/La ratios than MORB, probably indicating a melting source different from that of MORB. Data source: E-MORB and N-MORB (Sun and McDonough, 1989); BRP (Hawkesworth et al., 1995); orogenic andesites (Gill, 1981). Symbols as in Fig. 3.

(Table 2). Group 1 spans an $^{87}Sr/^{86}Sr$ range of 0.705222–0.706073 and a $^{143}Nd/^{144}Nd$ range of 0.512523–0.512621; when $t = 135$ Ma, the initial $^{87}Sr/^{86}Sr$ ratio ranges from 0.70502 to 0.70572 and $\varepsilon_{Nd}(t)$ from −0.78 to +0.91. Group 2 spans an $^{87}Sr/^{86}Sr$ range of 0.705612–0.706065 and a $^{143}Nd/^{144}Nd$ range of 0.512621–0.512645; when $t = 127$ Ma, the initial $^{87}Sr/^{86}Sr$ ratio ranges from 0.70497 to 0.70518 and $\varepsilon_{Nd}(t)$ from +0.86 to +1.26. Group 3 spans an $^{87}Sr/^{86}Sr$ range of 0.714545–0.720923 and a $^{143}Nd/^{144}Nd$ range of 0.512558–0.512590; when $t = 116$ Ma, the initial $^{87}Sr/^{86}Sr$ ratio ranges from 0.70501 to 0.70635 and $\varepsilon_{Nd}(t)$ from −0.41 to +0.25. In the initial $^{87}Sr/^{86}Sr(i)$ vs. $\varepsilon_{Nd}(t)$ variation diagram (Fig. 8), all of the samples plot in a narrow band, overlapping the Sr and Nd isotopic data of Cenozoic calc-alkaline volcanic rocks in the BRP reported by Hawkesworth et al. (1995).

5. Discussion

The late Mesozoic volcanic rocks in the NDHM show systematic variations in major and trace element concentrations and have homogeneous Sr and Nd isotopic ratios. We ask: (1) Which magmatic processes control the geochemical evolution of the melts? (2) Are all three groups of rocks derived from similar primitive melts? (3) And, if so, what is the source for the primitive melts? (4) In addition, what causes the extensive melting that occurred in the NDHM during late Mesozoic?

5.1. Magma differentiation

Despite a wide spectrum of rock types for the late Mesozoic volcanics in the NDHM, their homogeneous Sr–Nd isotope data and systematic variations in major and trace elements imply that significant crustal contamination did not take place during melt ascent. For Group 1 rocks, mass balance considerations suggest that such features as high Ba/Nb and La/Nb ratios in the rocks cannot realistically be attributed to crustal contamination of MORB, or of low La/Nb magmas (e.g., Hawkesworth et al., 1995). High Ba/Nb and La/Nb ratios are thus widely ascribed to source characteristics of a continental mantle lithosphere. On the other hand, the homogeneous Sr and Nd isotopic ratios and weakly variable K_2O/TiO_2 (0.98–2.01) and K_2O/P_2O_5 (2.22–4.84) ratios suggest an insignificant role of crustal contamination during magma evolution. Group 2 trachytes that develop relatively less enriched Sr and higher Nd isotopic ratios than Group 1 cannot be explained by crust contamination. As shown in Fig. 9a,b,

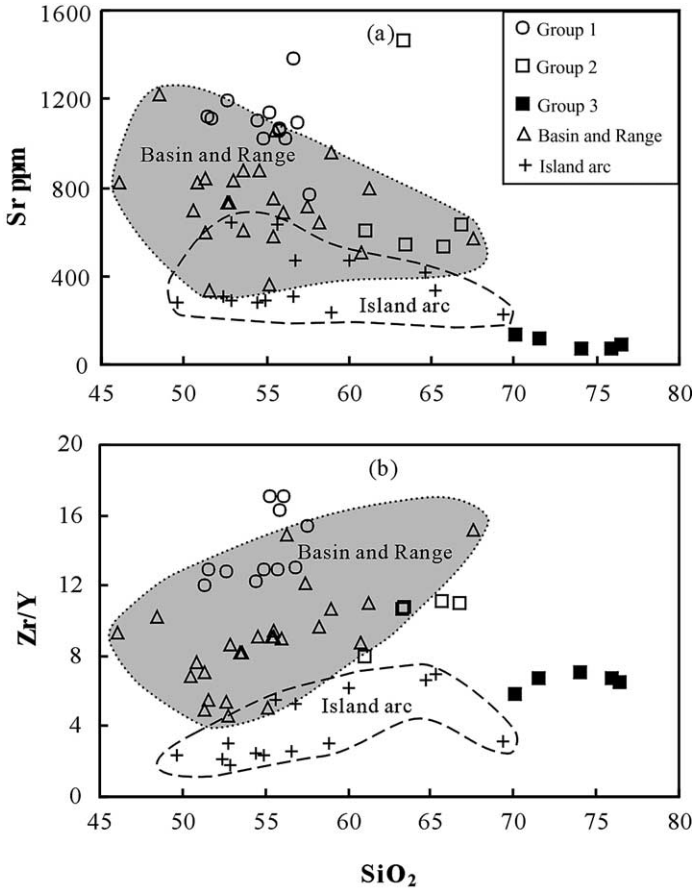

Fig. 7. A comparison of Sr content and Zr/Y ratio of the late Mesozoic volcanic rocks in the NDHM with those of Cenozoic volcanics in the BRP and island arc volcanics in Japan (Hawkesworth et al., 1995). Group 1 and Group 2 rocks possess similar Sr contents and Zr/Y ratios to those from BRP but higher than those from island arc volcanics. Symbols as in Fig. 3.

the slightly varied initial Sr and Nd isotopic ratios (initial $^{87}Sr/^{86}Sr = 0.70497–0.70635$; $\varepsilon_{Nd}(t) = -0.77$ to +1.26) from Group 1 through Group 2 to Group 3, indicate that Group 3 rhyolite lavas are probably highly fractional derivatives of the parental melts. On the other hand, mixing between two magma chambers could be an alternative process to generate the wide spectrum of rock types, but this possibility may be negligible as few enclaves were found.

The high SiO_2 and low MgO ($\leq 4.20\%$) contents of late Mesozoic rocks indicate that these rocks all are differentiates. A clear differentiation relationship among the three groups is suggested by the systematic variations in major and trace elements. With regard to typical intraplate and extension-related basalts (e.g., Smedley, 1986; Sun and McDonough, 1989; Hawkesworth et al., 1995; Rogers et al., 1995), Group 1 rocks show much lower MgO, FeO*, Ni and other compatible element concentrations. This means that these rocks were erupted to the surface after removal of Fe- and Mg-rich minerals such as olivine and orthopyroxene from the mantle-derived primary melts. Group 1 samples have the highest compatible element contents such as MgO, FeO* (total FeO), Ni, Sc, V, Co as well as the highest REE, Sr, and Ba concentrations, possibly representing the parental magmas from which Groups 2 and 3 were derived. Group 2 trachytes, which possess moderate MgO, FeO*, Ni, V, Co as well as Sr and Ba concentrations but the lowest

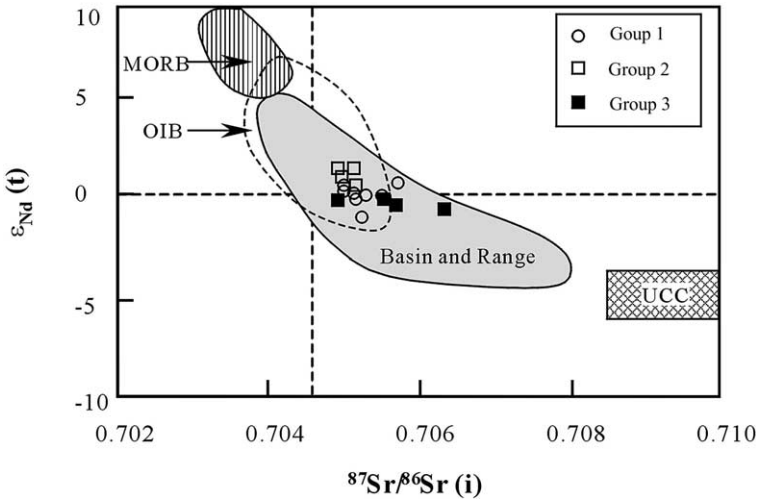

Fig. 8. $^{87}Sr/^{86}Sr(i)$ vs. $\varepsilon_{Nd}(t)$ plots of the late Mesozoic volcanics in the NDHM. All of the rocks exhibit slightly depleted to weakly enriched Nd isotopic ratios as well as slightly enriched Sr isotopic ratios, overlapping the variation range of the Cenozoic volcanic rocks in the BRP, USA (Hawkesworth et al., 1995; Rogers et al., 1995). UCC denotes the upper continental crust. Symbols as in Fig. 3.

REE, are produced after removal of feldspar and a few percent of LREE-rich minerals. Group 3 rhyolite lavas containing the lowest MgO, FeO*, Ni, V, Co, moderate REE and strongly negative Eu and Sr anomalies as well as the highest contents of strongly incompatible elements like K, Rb U, and Th, may represent the latest fractional melts after removal of most ferromagnesian phases and plagioclase.

The remarkable variation trend from Group 1 to Group 2 is that a rapid decrease in LREE (also MREE) occurs following magma evolution, which requires fractional crystallization of LREE- and MREE-rich minerals. It is generally suggested that hornblende is characterized by MREE enrichment and moderately enriched LREE contents. Additionally, it is also a major host for HFSE and V, whereas clinopyroxene and apatite are the major repositories of LREE, especially apatite in which the LREE contents can be thousands of times those of chondrite (Vannucci et al., 1991; Francis and Ludden, 1995; Ionov et al., 1997; O'Reilly and Griffin, 2000). Hornblende fractionation is predominant during magma evolution in accordance to the rapid decrease in MREE, V, Zr, TiO_2, FeO* (Figs. 4 and 5) and the obvious positive correlation between Zr and

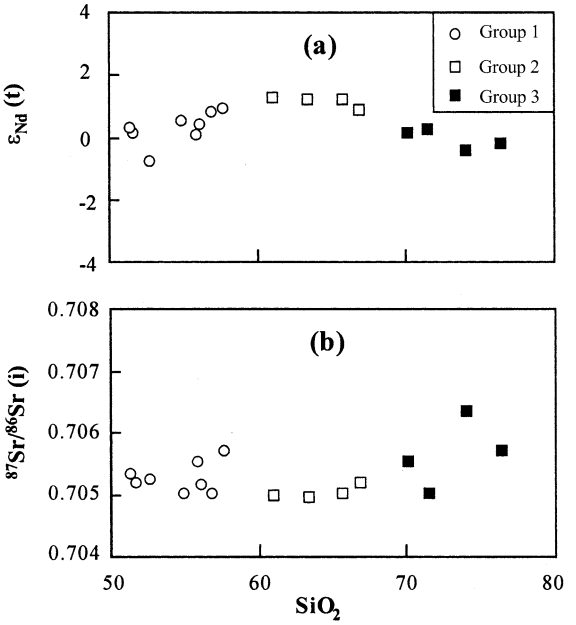

Fig. 9. Variation diagrams of initial $^{87}Sr/^{86}Sr$ isotopic ratio (a) and ε_{Nd} (b) with SiO_2 for the late Mesozoic volcanic rocks in the NDHM. Note that the slight variations in $^{87}Sr/^{86}Sr(i)$ and $\varepsilon_{Nd}(t)$ from Group 1 through Group 2 to Group 3 suggest an important role of FC process during magma evolution. Symbols as shown in the figure.

TiO_2, as shown in Fig. 10a. Due to moderate LREE contents in hornblende, removal of a few percent of hornblende could not lead to a rapid decrease in LREE; hence, other LREE-rich repositories must also be removed during magmatic evolution so as to generate the REE patterns in Group 2. As illustrated in Fig. 4, the negative covariation between SiO_2 and P_2O_5 implies that apatite was significantly fractionated. Further evidence from the obvious positive correlation between P_2O_5 and ΣREE content (Fig. 10b) also indicates an important role of apatite fractionation for the lowering of LREE contents from Group 1 to Group 2. Here, the maximum P_2O_5 decrease can be up to 0.63%, roughly equal to 1% of apatite being fractionated. Such an amount of apatite fractionation would lead to a decrease in LREE of tens to hundreds of ppm. On the other hand, a few percent of clinopyroxene fractionation is necessary to account for the lowering of CaO, Sr and LREE, whereas plagioclase fractionation is insignificant on the basis of the slight variation in Al_2O_3 and similar Eu anomalies.

Plagioclase-dominated fractionation is evident for Group 3 rhyolite lavas. For instance, these rocks show strongly negative Eu anomalies, negative correlation between Al_2O_3 and SiO_2 as well as significant Sr depletion in the PM-normalized spidergrams compared with Groups 1 and 2. Additionally, the negative correlation between Ba, Rb and SiO_2 observed in rhyolite lavas (Fig. 4j,k) also implies fractionation of a few biotites and alkali feldspars. Due to highly evolved affinity in Group 3, such as high SiO_2 (71.17–76.76%), K_2O (4.12–5.83% and $K_2O/Na_2O > 1.20$) and low MgO (0.41–1.0%) as well as moderate REE contents, at least two differentiation stages must be responsible for the generation of Group 3. The first stage was characterized by predominant fractionation of LREE-rich minerals such as hornblende, clinopyroxene and apatite to generate evolved melts like Group 2. The fractionated phases in the second stage was dominated by plagioclase as well as a few biotites and alkali feldspars, which had led to a rapid decrease in CaO, Al_2O_3, Sr, Ba, K, Rb and significantly negative Eu anomalies.

Overall, the parental magmas for the late Mesozoic volcanic rocks had undergone an extensive magmatic evolution, which can be described as the following sequence. Before eruption to the surface, strong olivine and pyroxene fractionation happened to form Group 1 rocks. The following fractional crystallization of hornblende (major)+clinopyroxene (a few percent)+apatite (about 1%) ± olivine (minor) from melts like Group 1 occurred to produce Group 2 trachytes, whereas the final plagioclase-predominant fractionation with minor biotite and alkali feldspar from melts like Group 2 took place to generate Group 3 rhyolite lavas.

5.2. Source characteristics

The slightly enriched Sr and weakly depleted to slightly enriched Nd isotopic ratios, significant LILE, LREE enrichment and strong Nb–Ta depletion observed in the Group 1, 2 and 3 rocks seem to favor a lithospheric mantle rather than depleted mantle reservoirs (e.g., asthenosphere or mantle plume) in their origin (Hawkesworth et al., 1995; Rogers et al., 1995; Guo et al., 2001). Nb–Ta depletion in mantle-derived melts is usually attributed to: (1) residual HFSE-rich minerals such as rutile, phlogophite, and amphibole during partial melting process; (2) crustal contamination during magma ascent; and (3) subduction-related metasomatism. It has been widely accepted that phlogophite and amphibole are unstable in convecting mantle and are first to be melted during magma generation (Olafsson and Eggler, 1983), so the possibility for residual phlogophite and amphibole can be negligible. Ionov et al. (1999) pointed out that rutile was usually generated during fluid/melt metasomatism in an off-cratonic lithosphere or an oceanic mantle reservoir to host Ti and other HFSE. Accordingly, if rutile had been retained in the melting sources after magma generation, then besides the Nb–Ta depletion, the primary melts derived from such mantle reservoirs should also have exhibited significantly negative Zr, Hf, and Ti anomalies. However, as observed in the PM-normalized spidergrams for Group 1 basaltic rocks (Fig. 5), these samples show no or insignificant Ti, Zr, and Hf anomalies, precluding the possibility for

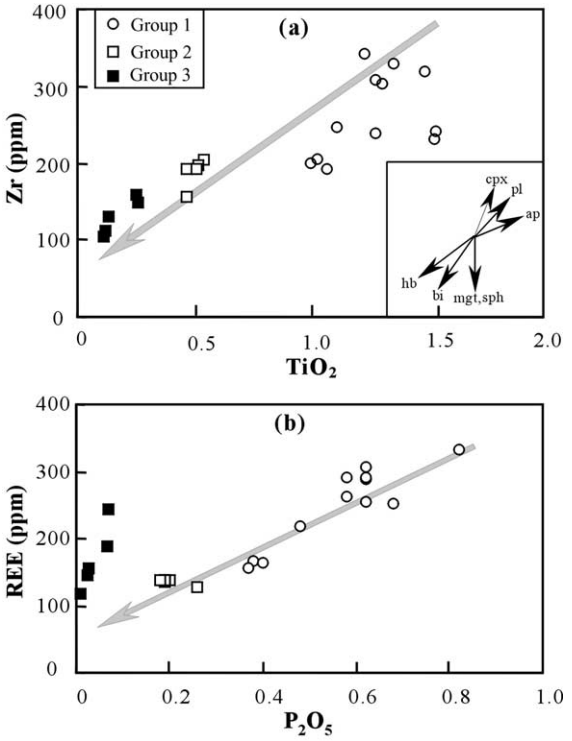

Fig. 10. Elemental variation diagrams of TiO_2 vs. Zr (a) and P_2O_5 vs. REE (b) for the late Mesozoic volcanics in the NDHM. Arrow indicates the magma evolution trend following an increase in SiO_2. In (a), hornblende fractionation is significant during magma evolution from Group 1 to Group 2. In (b), the positive correlation between P_2O_5 and REE contents suggests an important role of apatite fractionation for the lowering of REE concentrations from Group 1 to Group 2, while it is insignificant from Group 2 to Group 3. cpx, clinopyroxene; ap, apatite; sp, spinel; mgt, magnetite; hb, hornblende; bi, biotite; pl, plagioclase. Symbols as shown in the figure.

residual rutile in the melting source. As aforementioned, significant crustal contamination of MORB-like or other low La/Nb magmas could not well account for the geochemical and Sr–Nd isotope data. Probably, the observed Sr and Nd isotope ratios were mainly inherited from the melting source.

The spatial distribution of ophiolite suites and tectonic nappes indicates that multi-stage oceanic subduction occurred in the late Paleozoic (Sëngor et al., 1993; Sëngor and Natal'in, 1996; Robinson et al., 1999; Zhang and Zhou, 2001 and references therein). Dehydration of fluid-bearing minerals such as hornblende and chlorite will occur when oceanic crust and pelagic sediments are subducted. The released fluids are characterized by LILE and LREE enrichment relative to HFSE. These fluids metasomatize the overlying mantle peridotites, leading to LILE and LREE enrichment and HFSE depletion in the mantle reservoir. For instance, the very low Nb/Sr (0.004–0.012) and Nb/Ba (0.005–0.012) ratios and slightly enriched initial Sr isotopic ratios for Group 1 and Group 2 are likely to be a result of the involvement of a subduction component rather than a within-plate enrichment process (Ormerod et al., 1988). The strong U and Th enrichment in the spidergrams also favors a recent addition of pelagic sediments or altered oceanic crust in the melting source. However, geophysical and geological observations indicate that there did not exist contemporaneous oceanic plate subduction during the late Mesozoic (Engebretson et al., 1985; Li and Yang, 1987; Zhao and Coe, 1996). On the other hand, the higher Sr content and Zr/Y ratio of the late Mesozoic volcanics in the NDHM than those of typical island arc volcanics suggest an origin different from the metasomatized mantle wedge (Gill, 1981; Grove and Kinzler, 1986; Davies and Stevenson, 1992; Arculus, 1994; Hunter and Blake, 1995). All of these facts suggest that the primitive melts for late Mesozoic volcanics in the NDHM were derived from decompression melting of an enriched continental lithospheric mantle, which had been previously metasomatized by fluids derived from subducted slabs during the closure of the paleo-Asian and/or Mongolia–Okhotsk Oceans.

Rhyolite lavas can be produced either through remelting of lower mafic crust or fractional crystallization of mantle-derived melts (e.g., Borg and Clynne, 1998). Ge et al. (2000) noted that rhyolite lavas from the Da Hinggan Mountains could be grouped into two petrogenetic types. One type, containing relatively higher TiO_2 contents and high initial $^{87}Sr/^{86}Sr$ ratios (>0.710), was probably derived from remelting of lower/middle crust (Ge et al., 2001), whereas the low-TiO_2 type was formed through magma differentiation of the basaltic magmas. The low TiO_2 contents and initial Sr isotope ratios in Group 3 and the clear differ-

entiation relationship, as well as similar isotopic ratios to Groups 1 and 2, indicate that they probably represent the final differentiates rather than crustal remelting products.

5.3. Partial melting of lower lithosphere during post-orogenic extension

The origin and tectonic setting of the late Mesozoic volcanism in the NDHM have been long debated and three major viewpoints have been proposed (e.g., Jiang and Quan, 1988; Faure and Natal'in, 1992; Xia et al., 1993; Lin et al., 1998; Ge et al., 1999; Guo et al., 2001). The major controversy is focused on the following questions: (1) What kind of role did the interaction between the ancient Pacific Plate and the East Asian continental margin play in the formation of basin and range tectonics in NE China? (2) Could the extensive Mesozoic magmatism in NE China be regarded as a large igneous province (LIP) over a mantle plume? and (3) What was the relationship between lithospheric extension and large-scale calc-alkaline magmatism?

Lin et al. (1998) and Ge et al. (1999) noted that the extensive late Mesozoic magmatism in the Da Hinggan Mountains was induced by an upwelling mantle plume on the basis of the large-scale and multiple lithological associations of basaltic lavas. However, existence of an upwelling mantle plume is unlikely for the following reasons. Firstly, OIB-like basaltic rocks are lacking in the NDHM. Secondly, LIPs refer to voluminous ($10^6 km^3$ scale) magma generation and eruption within a few million years. Our K–Ar dating results and previous geochronological studies show that the voluminous calc-alkaline volcanism persisted for at least 20 Myr (BGMRNM, 1991, 1996; Ge et al., 2001). Thirdly, the upwelling of a mantle plume is generally associated with updoming of lithosphere and active rifting in the center of the rift zone (Trucotte and Emerman, 1983), whereas passive rifting is accompanied by subsidence and strong sedimentation (Smedley, 1986). The coeval basin and range tectonics and extensive sedimentation in the NDHM tend to confirm that passive lithospheric extension occurred during the late Mesozoic. Finally, the evolved affinities of the volcanic rocks in the NDHM suggested the existence of crustal magma reservoirs throughout the eruption episodes, in which the primary melts were strongly fractionated. In other words, the amount of lithospheric extension beneath the NDHM increased gradually rather than abruptly, and magmatism appears to have resulted from diffuse extension rather than rapid lithospheric thinning impacted by an upwelling mantle plume (Ruppel, 1995; Guo et al., 2001).

Undoubtedly, the East Asian continental margin has interacted with the circum-Pacific tectonic domain during late Mesozoic (Takahashi, 1983; Faure and Natal'in, 1992). However, the nature of the continental margin and the influence caused by interaction between the continental margin and the oceanic plate need to be further assessed. Previous studies have revealed that around the East Asian continental margin there existed an accretion melange belt along the Japan Sea, suggesting that the oceanic plate moved northward in a strike-slip way during the middle–late Jurassic to the early Cretaceous (Engebretson et al., 1985; Faure and Natal'in, 1992; Zhao et al., 1994). In other words, the contemporaneous oceanic subduction toward the East Asian continental margin was insignificant. Moreover, in the NDHM and Mongolia–Okhotsk orogenic belt, the late Mesozoic volcanism and rift-faulting basins extend westerly into eastern Mongolia, where the horizontal distance exceeds 1700 km from the East Asian continental margin. Hence, it is difficult to interpret the calc-alkaline magmatism and extensional tectonics as a consequence of the interaction between the East Asian continental margin and the subducted Izanagi or Kula Plate.

Hawkesworth et al. (1995) attributed the Cenozoic (>20 Ma) calc-alkaline magmatism in the BRP to lithospheric thinning and extension, which had triggered decompressional melting of the hydrous mantle lithosphere. Many similarities such as in the tectonic regime and magmatism are displayed between the BRP and the NE China fold belt, e.g., crustal extension and formation of rift-faulting basins as well as widely distributed calc-alkaline volcanism. This leads to an explanation for the extensive melting in terms of post-orogenic extension.

The widespread ophiolite suites and tectonic nappes in the NE China fold belt imply long-term plate subduction and continent–arc and/or microcontinent–continent collisions before the collision between the North China–Mongolian Block and the Siberia Craton (Robinson et al., 1999; Zhang and Zhou, 2001 and references therein). In the course of plate subduction, the overriding upper mantle peridotites had been metasomatized by fluids released from subducted slabs, leading to introduction of water and other volatiles to the mantle peridotite and lowering of its solidus (e.g., Gill, 1981; Arculus, 1994). After final closure of the Mongolia–Okhotsk Ocean and collision between the North China–Mongolian Block and the Siberia Craton in the middle Jurassic (Zhao et al., 1994; Zhao and Coe, 1996; van der Voo et al., 1999), the regional structural deformation style had transformed from the predominance of compression in the syn-tectonic stage into lithospheric extension during the post-orogenic stage. Extensional tectonics in orogenic belts usually develop during the post-orogenic stage in response to readjustment of the thickened lithosphere or lithospheric thinning by means of mantle convection, lithospheric collapse, slab breakoff and/or detachment (England and Houseman, 1989; Platt and England, 1994; Ruppel, 1995; Davis and von Blanckenburg, 1995). When the amount of extension, or thinning factor β, is enough to make the geotherm graze the solidus, decompressional melting will take place (McKenzie and Bickle, 1988; Daley and DePaolo, 1992; Turner et al., 1996; Miller et al., 1999).

The development of typical intracontinental extensional tectonics, fault-rifting basins (Li and Yang, 1987), and extensive calc-alkaline magmatism suggest that post-orogenic extension was predominant in the NDHM during late Mesozoic. Following the lithospheric extension and/or orogenic collapse, passive rifting and asthenospheric upwelling occurred (Shao et al., 1994, 1998), which induced geothermal elevation from a cold and thickened lithosphere to a hot and rift-related one. Due to lower solidus of hydrous peridotites, decompressional melting of the lower enriched lithospheric mantle produced the primitive melts. In the crustal magma reservoirs, the primary melts had experienced a different degree of fractionation to form the wide spectrum of rock types with voluminous mafic cumulates retained in the crust. This is in good agreement with the seismic investigations that beneath the NE China fold belt there exist several km-thick low-velocity layers within the crust (Yuan, 1996).

6. Concluding remarks

The late Mesozoic volcanism in the NDHM is characterized by significant LILE and LREE enrichment but HFSE depletion with a little enriched to slightly depleted Nd and weakly enriched Sr isotope ratios. The rocks generally display similar geochemical and isotopic characteristics to Cenozoic calc-alkaline rocks of the BRP, and show higher Sr contents and Zr/Y ratios compared with island arc volcanics. Group 1 rocks of the Tamulangou Fm. were derived from a lithospheric mantle metasomatized by fluid released from subducted slabs during Paleozoic–early Mesozoic time, when closure of the paleo-Asian and Mongolia–Okhotsk Oceans took place. Decompressional melting of such metasomatized mantle reservoirs and early differentiation of ferromagnesian minerals of the primitive magmas can account for their genesis. Group 2 trachytes of the Jixiangfeng Fm. were generated by fractionation of the parental melts (like Group 1) after removal of LREE-rich minerals such as hornblende and clinopyroxene, as well as minor apatite. Group 3 rhyolite lavas of the Shangkuli Fm. represent the final differentiates after a plagioclase-predominant fractionation.

The low MgO and high SiO_2 contents of the rocks and clear differentiation relationship among Groups 1, 2 and 3 imply the existence of crustal magma reservoirs beneath the NDHM throughout the whole eruption sequence. Due to their distinguishable geochemical features from island arc volcanics and LIPs, the late Mesozoic calc-alkaline volcanism in the NDHM and contemporaneous basin and range tectonics are attributed to post-orogenic diffuse extension rather than either an upwelling mantle plume or Mesozoic oceanic subduction of the ancient Pacific plate.

Acknowledgements

The authors would like to thank Ms. Y. Liu for her assistance in performing ICP-MS trace element analysis and senior technicians G.S. Qiao and R.H. Zhang for Sr and Nd isotopic analysis. Z.P. Pu is thanked for K–Ar dating. Thorough and helpful reviews by Dr. R.C. Bacon and F.Y. Wu have significantly improved the manuscript. Dr. Weaver is thanked for his effort in editing the paper. This study was financially supported by the Chinese Academy of Sciences (No. KZCX2-104).

References

Arculus, R.J., 1994. Aspects of magma genesis in arcs. Lithos 33, 189–208.

Borg, L.E., Clynne, M.A., 1998. The petrogenesis of felsic calc-alkaline magmas from the southernmost Cascades, California: origin by partial melting of basaltic lower crust. J. Petrol. 39, 1197–1222.

Bureau of Geology and Mineral Resources of Nei Mongol Autonomous Region (BGMRNM), 1991. Regional Geology of Nei Mongol Autonomous Region. Geological Publishing House, Beijing, 725 pp. (in Chinese).

Bureau of Geology and Mineral Resources of Nei Mongol Autonomous Region (BGMRNM), 1996. Stratigraphy of Nei Mongol Autonomous Region. China University of Geoscience Press, 344 pp. (in Chinese).

Chen, B., Jahn, B.M., Wilde, S., Xu, B., 2000. Two contrasting Paleozoic magmatic belts in northern Inner Mongolia, China: petrogenesis and tectonic implications. Tectonophysics 328, 157–182.

Daley, E.E., DePaolo, D.J., 1992. Isotopic evidence for lithospheric thinning during extension: Southeastern Great Basin. Geology 20, 104–108.

Davies, J.H., Stevenson, D.J., 1992. Physical model of source region of subduction zone volcanics. J. Geophys. Res. 97, 2037–2070.

Davis, J.H., von Blanckenburg, F., 1995. Slab breakoff: a model of lithosphere detachment and its test in the magmatism and deformation of collisional orogens. Earth Planet. Sci. Lett. 129, 327–343.

Engebretson, D.C., Cox, A., Gordon, R.G., 1985. Relative motions between oceanic and continental plates in the Pacific basins. Geol. Soc. Am. Spec. Publ., 206, pp. 1–59.

England, P.C., Houseman, G.A., 1989. Extension during continental convergence, with application to the Tibet Plateau. J. Geophys. Res. 94, 17561–17579.

Fan, W.M., Guo, F., Wang, Y.J., Lin, G., Zhang, M., 2001. Post-orogenic bimodal volcanism along the Sulu Orogenic Belt in eastern China. Phys. Chem. Earth A 26, 733–746.

Faure, M., Natal'in, B., 1992. The geodynamic evolution of the eastern Eurasian margin in Mesozoic times. Tectonophysics 208, 397–411.

Francis, D., Ludden, J., 1995. The significance of hornblende in mafic alkaline lavas, a study in the northern Canadian Cordillera. J. Petrol. 38, 1171–1191.

Ge, W.C., Lin, Q., Sun, D.Y., Wu, F.Y., Won, C.K., Lee, M.W., Jin, M.S., Yun, S.K., 1999. Geochemical characteristics of Mesozoic basaltic volcanic rocks in the Da Hinggan Mts: evidence for mantle-crust interaction. Acta Petrol. Sin. 15, 396–407 (in Chinese with English abstract).

Ge, W.C., Lin, Q., Sun, D.Y., Wu, F.Y., 2000. Geochemical study on of the two types of Mesozoic rhyolite lavas in the Da Hinggan Mts. Earth Sci. J. China Univ. Geosci. 25, 172–178 (in Chinese with English abstract).

Ge, W.C., Li, X.H., Lin, Q., Sun, D.Y., Wu, F.Y., Yun, S.H., 2001. Geochemistry of early Cretaceous alkaline rhyolites from Hulun Lake, Da Hingan Mts and its tectonic implications. Chin. J. Geol. 36, 176–183 (in Chinese with English abstract).

Gill, J.B., 1981. Orogenic Andesites and Plate Tectonics. Springer Verlag, New York, 385 pp.

Grove, T.L., Kinzler, R.J., 1986. Petrogenesis of andesites. Annu. Rev. Earth Planet. Sci. Lett. 14, 417–454.

Guo, F., Fan, W.M., Wang, Y.J., Lin, G., 2001. Petrogenesis of the late Mesozoic bimodal volcanic rocks in the southern Da Hinggan Mts, China. Acta Petrol. Sin. 17, 161–168 (in Chinese with English abstract).

Han, B.H., Wang, S.G., Jahn, B.M., Hong, D.W., Kagami, H., Sun, Y.L., 1997. Depleted-mantle source for the Ulungur River A-type granites from North Xinjiang, China: geochemistry and Nd-Sr isotopic evidence, and implications for Phanerozoic crustal growth. Chem. Geol. 138, 135–159.

Hawkesworth, C.J., Turner, S., Gallagher, K., Hunter, A., Bradshaw, T., Rogers, N., 1995. Calc-alkaline magmatism, lithospheric thinning and extension in the Basin and Range. J. Geophys. Res. 100, 10271–10286.

Hong, D.W., Hunag, H.Z., Xiao, Y.J., Xu, H.M., Jin, M.Y., 1994. Petrogenesis of Permian alkaline granites in central Inner Mongolia Autonomous Region and geodynamic significance. Acta Geol. Sin. 68, 219–230 (in Chinese with English abstract).

Hooper, P.R., Bailey, D.G., McCarley Holder, G.A., 1995. Tertiary calc-alkaline magmatism associated with lithospheric extension in the Pacific Northwest. J. Geophys. Res. 100, 10303–10319.

Hunter, A.G., Blake, S., 1995. Petrogenetic evolution of a transitional tholeiitic-calc-alkaline series: Towada volcano, Japan. J. Petrol. 36, 1579–1605.

Ionov, D.A., Gregoire, M., Prikhod'ko, V.S., 1999. Feldspar-Ti-oxide metasomatism in off-cratonic continental and oceanic upper mantle. Earth Planet. Sci. Lett. 165, 37–44.

Ionov, D.A., O'Reilly, S.Y., Griffin, W.L., 1997. Volatile-bearing minerals and lithophile trace elements in the upper mantle. Chem. Geol. 141, 153–184.

Irvine, T.N., Baragar, W.R.A., 1971. A guide to the chemical

classification of the common volcanic rocks. Can. J. Earth Sci. 8, 523–528.

Jahn, B.M., Wu, F.Y., Lo, C.-H., Tsai, C.H., 1999. Crust-mantle interaction induced by deep subduction of the continental crust: Geochemical and Sr-Nd isotopic evidence from post-collisional mafic-ultramafic intrusions of the northern Dabie complex, central China. Chem. Geol. 157, 119–146.

Jiang, G.Y., Quan, H., 1988. Mesozoic volcanic rocks of Genhe and Hailar basins in Da Hinggan Mountains. J. Shenyang Inst. Geol. Miner. Source Chin. Acad. Geol. Sci. 3, 23–100 (in Chinese).

Kuzmin, M.L., Abramovich, G.Y.A., Dril, S.L., Kravchinsky, V.Y.A., 1996. The Mongolian-Okhotsk suture as the evidence of late Paleozoic-Mesozoic collisional processes in Central Asia. Abstract of 30th IGC, Beijing, Vol. 1, p. 261.

Le Bas, M., Le Maitre, R.W., Streckeisen, A., Zanettin, B., 1986. A chemical classification of volcanic rocks based on the total-silica diagram. J. Petrol. 27, 745–750.

Liegéois, J-P., Navez, J., Hertogen, J., Black, R., 1998. Contrasting origin of post-collisional high-K calc-alkaline and shoshonitic versus alkaline and peralkaline granitoids. The use of sliding normalization. Lithos 45, 1–28.

Lin, Q., Ge, W.C., Sun, D.Y., Wu, F.Y., Won, C.K., Min, K.D., Jin, M.S., Lee, M.W., Kwon, C., Yun, S., 1998. Tectonic implications of Mesozoic volcanic rocks in Northeastern China. Sci. Geol. 33, 129–139 (in Chinese with English abstract).

Li, S.T., Yang, S.G., 1987. The late Mesozoic rifting in the northeastern China and the fault-rifting basins in East Asia. Sci. China Ser. B 21, 185–195.

Liu, Y., Liu, H.C., Li, X.H., 1996. Simultaneous and precise determination of 40 trace element elements using ICP-MS. Geochimica 25, 552–558 (in Chinese with English abstract).

McKenzie, D.P., Bickle, M.J., 1988. The volume and composition of melt generated by extension of the lithosphere. J. Petrol. 32, 625–679.

Miller, C., Schuster, R., Klotzli, U., Frank, W., Purtscheller, F., 1999. Post-collisional potassic and ultrapotassic magmatism in SW Tibet: geochemical and Sr-Nd-Pb-O isotopic constraints for mantle source characteristics and petrogenesis. J. Petrol. 40, 1399–1424.

Olafsson, M., Eggler, D.H., 1983. Phase relations of amphibole, amphibole-carbonate, and phlogopite-carbonate peridotite: petrologic constraints on the asthenosphere. Earth Planet. Sci. Lett. 64, 305–315.

Ormerod, D.S., Hawkesworth, C.J., Rogers, N.W., Leeman, W.P., Menzies, M.A., 1988. Tectonic and magmatic transitions in the Western Great Basin, U.S.A.. Nature 333, 349–353.

O'Reilly, S.Y., Griffin, W.L., 2000. Apatite in the mantle: implications for metasomatic processes and high heat production in Phanerozoic mantle. Lithos 53, 217–232.

Platt, J.P., England, P.C., 1994. Convective lithospheric thinning beneath mountain belts: thermal and mechanical consequences. Am. J. Sci. 294, 349–353.

Robinson, P.T., Zhou, M., Hu, X., 1999. Geochemical constraints on the origin of the Hegenshan Ophiolite, Inner Mongolia, China. J. Asian Earth Sci. 17, 423–442.

Rogers, N.W., Hawkesworth, C.J., Ormerod, D.S., 1995. Late Cenozoic basaltic magmatism in the Western Great Basin, California and Nevada. J. Geophys. Res. 100, 10287–10301.

Rotturaa, A., Bargossia, G.M., Caggianellib, A., Del Moroc, A., Visonàd, D., Trannea, C.A., 1998. Origin and significance of the Permian high-K calc-alkaline magmatism in the central-eastern Southern Alps, Italy. Lithos 45, 329–348.

Ruppel, C., 1995. Extensional processes in continental lithosphere. J. Geophys. Res. 100, 24187–24215.

Sëngor, A.M.C., Natal'in, B.A., Burtman, V.S., 1993. Evolution of the Altaid tectonic collage and Paleozoic crustal growth in Eurasia. Nature 364, 299–307.

Sëngor, A.M.C., Natal'in, B.A., 1996. Paleotectonics in Asia: fragments of a synthesis. In: Yin, A. et al. (Eds.), The Tectonic Evolution of Asia. Cambridge University Press, Cambridge, pp. 486–640.

Shao, J.A., Zang, S.X., Mou, L.Q., 1994. Extensional tectonics and asthenospheric upwelling in the orogenic belt: a case study from Hinggan-Mongolia Orogenic belt. Chin. Sci. Bull. 39, 533–537.

Shao, J.A., Zhang, L.Q., Mou, B.L., 1998. Tectono-thermal evolution of the middle-south section of Da Hinggan Mountains. Sci. China Ser. D 28, 193–200.

Smedley, P.L., 1986. The relationship between calc-alkaline volcanism and within-plate continental rift volcanism: evidence from Scottish Palaeozoic lavas. Earth Planet. Sci. Lett. 76, 113–128.

Sun, S.S., McDonough, W.F., 1989. Chemical and isotopic systematics of oceanic basalts: implication for mantle composition and processes. In: Saunder, A.D., Norry, M.J. (Eds.), Magmatism in the Ocean Basins. Geol. Soc. Spec. Publ., 42, pp. 313–345.

Takahashi, M., 1983. Space-time distribution of late Mesozoic to early Cenozoic magmatism in East Asia and its tectonic implications. In: Takahashi, M. (Ed.), Accretion Tectonics in the Circum-Pacific Regions. Terra Publ., Tokyo, pp. 69–88.

Taylor, S.R., McLennan, S.M., 1985. The Continental Crust: Its Composition and Evolution. Blackwell, Oxford, 312 pp.

Trucotte, D.L., Emerman, S.H., 1983. Mechanisms of active and passive rifting. Tectonophysics 94, 39–50.

Turner, S., Arnaud, N., Liu, J., Hawkesworth, C.J., Harris, N., Kelley, S., van Calsteren, P., Peng, W., 1996. Post-collision, shoshonitic volcanism on the Tibetan Plateau: implications for convective thinning of the lithosphere and the source of oceanic basalts. J. Petrol. 37, 45–71.

van der Voo, R., Spakman, W., Bijwaard, H., 1999. Mesozoic subducted slabs under Siberia. Nature 397, 246–249.

Vannucci, R., Tribuzio, R., Piccardo, G.B., Ottolini, L., Bottazzi, P., 1991. SIMS analysis of REE in pyroxenes and hornblendes from the Proterozoic Ikasaulak intrusive complex (SE Greenland): implications for LREE enrichment processes during post-orogenic plutonism. Chem. Geol. 92, 115–133.

Wu, F.Y., Jahn, B.M., Lin, Q., 1997. Sr, Nd and Pb isotopic

compositions of post-orogenic granites in the northern China Orogen and its implications for continental crustal growth. Chin. Sci. Bull. 42, 2188–2192.

Wu, F.Y., Jahn, B.M., Wilde, S., Sun, D.Y., 2000. Phanerozoic crustal growth: U-Pb and Sr-Nd isotopic evidence from the granites in northeastern China. Tectonophysics 328, 89–113.

Xia, J., Wang, C.S., Li, X.H., 1993. Geochemical characteristics of the Mesozoic volcanic rocks in Hailar basin and its adjacent areas and discussion on volcanic rocks of marginal block type. J. Chengdu Coll. Geol. 20, 67–79 (in Chinese).

Yuan, X.C., 1996. Atlas of geophysics in China. In: Yuan, X.C. (Ed.), Geophysical Map Collections in China. Geological Press, Beijing, pp. 59–62 (in Chinese).

Zhang, Q., Zhou, G.Q., 2001. Ophiolites of China. Science Press, Beijing, 182 pp. (in Chinese).

Zhao, G.L., Yang, G.L., Fu, J.Y., 1989. Mesozoic volcanic rocks in the central-southern Da Hinggan Mts. Beijing Press of Science and Technology, Beijing, 155 pp. (in Chinese).

Zhao, X.X., Coe, R.S., 1996. Paleomagnetic constraints on the paleogeography of China: implications for Gondwanaland. Abstract of 30th IGC, Beijing, Vol. 1, p. 231.

Zhao, X.X., Coe, R.S., Zhou, Y.S., Wu, H.R., Wang, J., 1990. New palaeomagnetic results from northern China: collision and suturing with Siberia and Kazakhstan. Tectonophysics 181, 43–81.

Zhao, Y., Yang, Z., Ma, X., 1994. The important age of tectonic transformation from paleo-Asian to the Pacific tectonic domains in the East Asia. Sci. Geol. Sin. 29, 105–119 (in Chinese with English abstract).